DESIGN OF A SUPERFERRIC DIPOLE FOR THE SUPERCONDUCTING SUPERCOLLIDER*

H. Bingham
R. Carcagno
M. Davidson
H. Hinterberger
F. R. Huson
M. Kobayashi

W. W. MacKay
S. Pissanetzky
R. Rocha
W. Schmidt
R. Stegman

Texas Accelerator Center
2319 Timberloch Place
The Woodlands, Texas 77380
U.S.A.

RESUMEN

El SSC es un acelerador de protones de dos haces de 20 TeV cada uno, que utiliza electroimanes superconductores y cuya construccion commenzara en 1987. El Texas Accelerator Center esta desarrollando el diseno de electroimanes superferricos para el SSC. El dipolo superferrico consiste de un nucleo de hierro laminado excitado por unas pocas espiras de superconductor. La longitud mangetica de cada dipolo es de 105m, el entrehierro es de 2.5 x 3.7 cm, y el campo es uniforme dentro de una parte en 10^4 para un rango dinamico desde 0.15T para inyeccion a 1 TeV, hasta 3T para almanceamiento a 20 TeV. Dos imanes, uno para cada haz, van intalados en un mismo criostato. El acelerador necesita 1000 dobles dipoles.

Aqui presentamos la version de hierro frio del dipolo superferrico. Discutimos el diseno basico, el diseno del superconductor y su aislacion, la calidad y extension del campo uniforme, las fuerzas magneticas y la energia almacenada, las tolerancias y errores para la produccion en gran escala, y los resultados de mediciones en varios prototipos. Tambien describimos los programas de diferencias finitas y de elementos finitos usados para el diseno.

ABSTRACT

The Superconducting Supercollider (SSC) is a 20TeV on 20Tev dual beam proton accelerator, which will use superconducting magnets and whose construction is expected to begin in 1987. The Texas Accelerator Center is pursuing the superferric option for the SSC reference design. The superferric dipole magnet consists of a laminated iron yoke powered by a few turns of superconductor. These dipoles have a magnetic length of 105m and a bore of 2.5cm x 3.7cm and have been designed to produce a field uniform to 1 part in 10^4, for fields from 0.15T at an injection energy of 1TeV to 3T at a storage energy of 20TeV. Two such magnets, one for each beam, are placed in a single cryostat. The accelerator will require approximately 1,000 double dipoles. We present the cold iron version of the superferric dipole. We discuss its basic design, the design of the superconductor and its insulation, the good field size and quality, the magnetic forces and stored energy, the dimensional tolerances and errors for industrial production, and test results of several prototypes. We also describe the finite difference and finite element computer software used for the design.

INTRODUCTION

The design of the Superconducting Supercollider (SSC) was chartered in December, 1983, by the directors of the U.S. high energy accelerator laboratories. The purpose of the National SSC Reference Design Study was to review all technical and economic details of various options for creating the SSC, a 20 TeV on 20 TeV proton-proton collider with a luminosity of up to $10^{33} cm^{-2} sec^{-1}$.

The study contemplates three different styles of superconducting magnets, each emphasizing a different idea aimed at reducing the final cost of the accelerator. The Texas Accelerator Center is pursuing the superferric magnet option for the SSC, in its cold iron version. [1]A superferric magnet is driven by a few turns of superconductor, but its field is dominated by iron. The iron yoke and pole tips are refrigerated at liquid helium temperature. Superferric magnets are characterized as follows:

(i) Low current. Since the field is iron-dominated the current is minimized. Forces and stored energy are lower by an order of magnitude than those for coil dominated magnets. The effects of persistent currents and field errors due to coil misplacement are also minimized.

(ii) Simple and reliable. Since the current is low and there are only 10 turns of flat superconductor placed against the surface of the steel, the magnets are very simple to construct and operate. Industrial production of large quantities of these magnets is possible, as has

already been confirmed by industry. Reliability has also
proved to be very good.

(iii) Inexpensive. Experience with the Energy Doubler
indicates that the dominant costs of a magnet are the
superconductor and the ends (labor, bellows, welds, etc.)
Superferrics have 1/4 or less superconductor than normal
superconducting magnets. Besides superferric magnets are
very long. Each magnet consists of three sections, each
35m long, welded together and placed in the same cryostat,
so that end cost is minimized.

Of course, superferric magnets have the disadvantage
of a lower field, and thus a larger radius machine.

Historically, several versions of the 3T superferric
magnet with 2.5 cm bore were considered by TAC. They are:

Crenellated superferrics - Crenellated magnets can be used
to generate a uniform field [2]. However, a later study [3]
showed that crenellation is not feasible for 3T
superferrics, and the idea was abandoned.

NF2C (Narrow Face with 2 Currents) - This was the first
design with flat pole tips and two independent coils. The
sum of the two currents determines the field B_0 in the
bore, while their ratio controls the sextupole harmonic
coefficient b_2 and can be adjusted to improve the
uniformity of the field. This design showed the need of
using a wider pole face.

WF2C (Wide face with 2 Currents) - This design works
under the same priciples as the NF2C and is schematically
shown in Figure 1. Models of WF2C were built and many
calculations and measurements were made. This design
gives the desired B_0, and b_2 can be made zero, but the
decapole b_4 is somewhat larger than what we would like,
particularly at high field. This design was discontinued.

WF3CMS (Wide face with 3 currents and a magnetic shunt).
This design has two independent main coils of 4 turns each
plus a third small correction coil with only 2 turns,
Figures 2 and 3. The ratio of the two main currents is
used to zero the sextupole b_2, and the correction current
to make the decapole b_4 equal to zero. A magnetic shunt
is also incorporated. The shunt consists of a steel
lamination the same kind as used for the yoke, placed flat
against the inside of the main coils. The shunt has a
small effect on B_0 , but it has the following favorable
effects. The field at the superconductor becomes smaller,
and the critical current becomes larger, so that more
current can be used without the risk of quench. Field
errors due to conductor misplacement become smaller
because coils can be more accurately placed with the help
of the shunt. The shunt provides additional shielding
against the effect of persistent current. It also serves
to protect the coils during assembly. The undesirable

effects of remanent fields at injection are minimized.
None of these, however, was the real reason for
introducing the shunt. The real reason was that with the
help of the shunt the field becomes more uniform, and b_2
and b_4 become easier to zero with the current ratios.
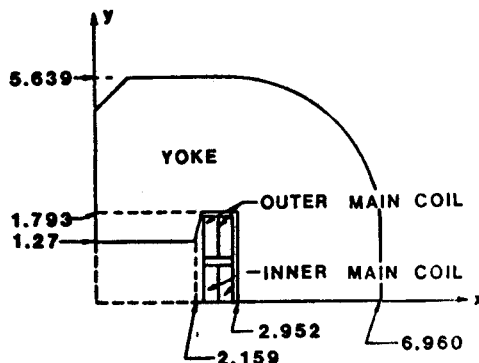
Figure 1. Geometry of the WF2C superferric design.
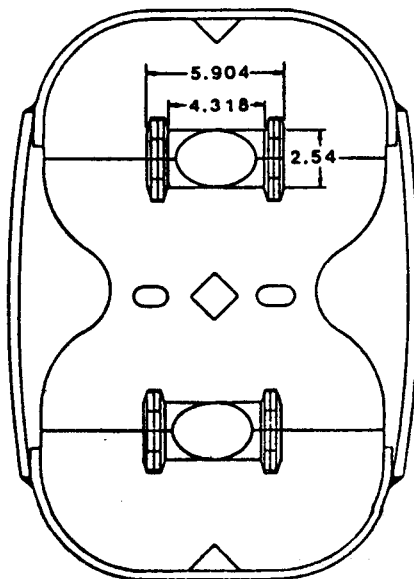
Figure 2. The WF3CMS superferric design
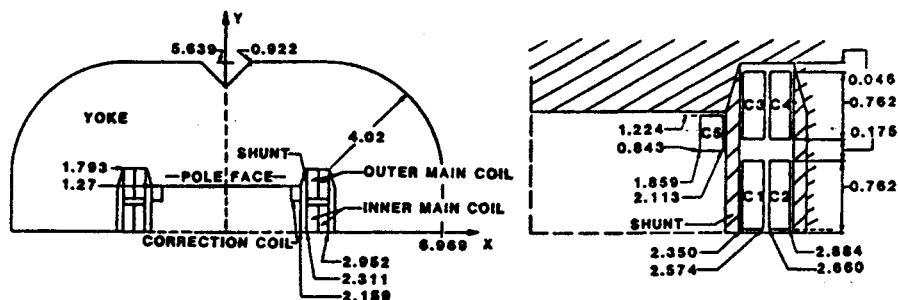
Figure 3. Geometry of the WF3CMS superferric design.

A few models of WF3CMS were built, including one by industry. Measurements and calculations were made and are reported here. WF3CMS is a working design.

Table I illustrates the prototypes built to date and their designations. We discuss the design of the superconductor, the quality of the predicted field, the magnetic forces and stored energy, the construction errors for industrial production, and test results for several prototypes of both the WF2C and WF3CMS types.

Table I. Superferric prototypes built to date (August 1985)

DESIGNATION	TYPE	LENGTH	BORES IN CRYOSTAT	MANUFACTURER
TAC1	NF2C	1m	1	TAC
TAC2	NF2C	1m	1	TAC
TAC3	WF2C	8m	2	TAC
TAC4	WF2C	1m	2	TAC
TAC5	WF3CMS	1m	1	TAC
GD1	WF3CMS	1m	1	General Dynamics
TAC6	WF3CMS	1m	2	TAC
TAC7	WF3CMS	1m	1	TAC
TAC9	WF3CMS	1m	1	TAC
TAC10	WF3CMS	1m	1	TAC

THE CONDUCTOR

The conductor proposed for the superferric magnet is the ''Energy Doubler low-β conductor'' see figure 4. The 0.0681cm diameter strands of the conductor are a composite

of superconductor filaments in a high conductivity copper
matrix with a Cu/S.C. =1.3. The superconductor alloy
composition is Nb46.5 weight % Ti and is a high
homogeneity grade. The use of high homogeneity material
will yield current densities of up to 20% greater than
conventional material. The superconductor filament size
was chosen to be in the 15-20 μm range for ease of
manufacturing. The main coil conductor is made of 24
strands, whereas the trim coil conductor is made of 12
strands. Typical strand critical current density values
are in the range $J_c(3T, 4.2K, \rho=10^{-12}\Omega-cm) \cong 4000A/mm^2$ and
typical cable critical current values are $I_c \cong 15,000A$
under the same test conditions. Measurements of critical
currents are shown in Figures 5 and 6.

MAIN COIL CONDUCTOR

KAPTON — INSULATION
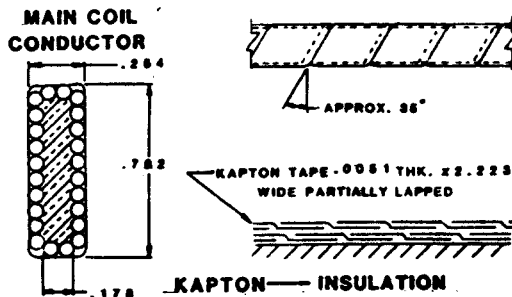
Figure 4.   The superconductor used for superferric
magnets.
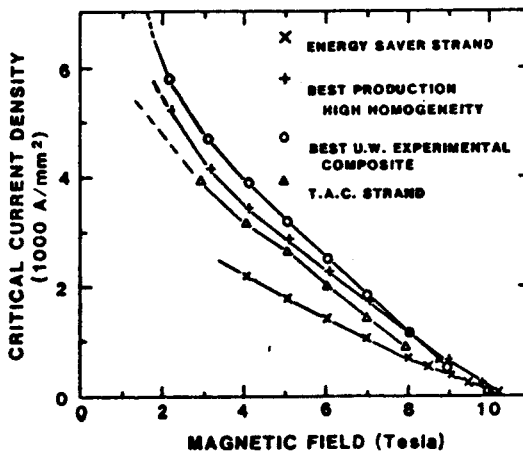
Figure 5.   Comparison of critical current density of TAC
strand to that of other conductors.
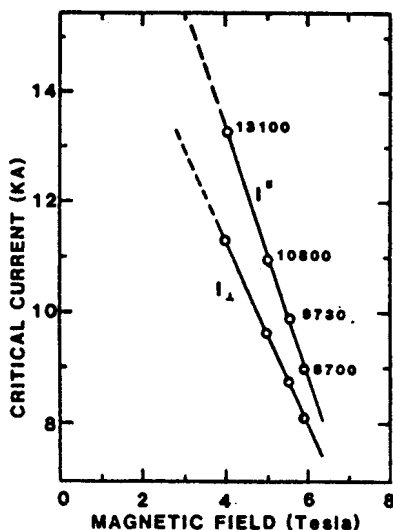
Figure 6. Measurements of cable critical current.

FIELD AND MULTIPOLE CALCULATIONS

In two dimensions, the magnetic induction can be expanded in multipoles:

$$B_x = B_0 \sum_{n=1} (r/R)^n (b_n \sin n0 + a_n \cos n0)$$

$$B_y = B_0 \left(1 + \sum_{n=1} (r/R)^n (b_n \cos n0 - a_n \sin n0)\right)$$

where B_x and B_y are, respectively, the horizontal and vertical components of the magnetic induction at x = r cos 0, y = r sin 0, and B_0 is the magnetic induction at the origin, assumed to have only y component. The relative strengths of the multipoles are: b_n for the normal multipole and a_n for the skew multipoles. All multipole coefficients are dimensionless. R is the normalization radius, taken as 1 cm for all our work.

The field and multipole calculations were performed using the well-known finite difference program POISSON after the large errors observed in this program[7] have been corrected [8]. Only results pertaining to the WF3CMS version are given. The design goals call for all normalized multipole coefficients to be below 2 parts in 10^4 at a radius of 1 cm for fields ranging from 0.15 Tesla to 3.00 Tesla. Table II shows that this goal has been met.

The geometry of the WF3CMS magnet is shown in figure 3. I_{in} and I_{out} provide most of the excitation for B_0, while their ratio controls the sextupole b_2. I_c is normally much smaller in magnitude and provides the correction for the decapole b_4. The excitation currents are plotted against B_0 in figure 7. The very small values

of I_{out} in the vicinity of 2.2 Tesla have prompted yet another slight change in the geometry. The inner currents I_{in} have been moved onto the midplane from their present location 0.61 cm above it. This has the effect of increasing I_{out} and decreasing I_{in} in this region. At this time detailed predictions for the entire range are not available, however, the ability to control the sextupole and decapole will remain the same. Only the currents and ratios will shift slightly.

Because the model was perfectly symmetric the predicted skew multipoles are zero as are the odd b coefficients . The currents in table II are in amperes, B_0 in Tesla and the other b coefficients are in parts in 10^4.

Table II. Predicted Fields and Multipoles

$B_0(T)$	$I_{in}(A)$	$I_{out}(A)$	$I_c(A)$	b_2	b_4	b_6	b_8
0.1520	678.0	0.0	182.0	-0.92	0.20	0.60	0.26
0.5041	2160.0	190.0	400.0	0.00	0.54	0.60	0.26
0.8303	3525.0	375.0	600.0	0.10	0.58	0.59	0.23
1.2108	5120.0	490.0	900.0	-0.59	-0.42	0.45	0.11
1.6274	7200.0	500.0	1200.0	-0.72	2.10	1.70	0.31
1.8832	8500.0	300.0	1700.0	-0.75	1.18	0.97	0.19
2.0397	9420.0	30.0	2100.0	-0.33	1.70	1.15	0.20
2.2789	10650.0	15.0	2700.0	-0.02	1.95	1.08	0.18
2.3100	10850.0	0.0	2950.0	-0.68	0.82	0.90	0.33
2.3600	10975.0	425.0	2750.0	-0.34	0.72	0.93	0.32
2.7970	11650.0	6150.0	-500.0	-0.37	0.42	2.06	0.39
2.9889	11500.0	10000.0	-2400.0	-0.04	-0.97	2.12	0.47
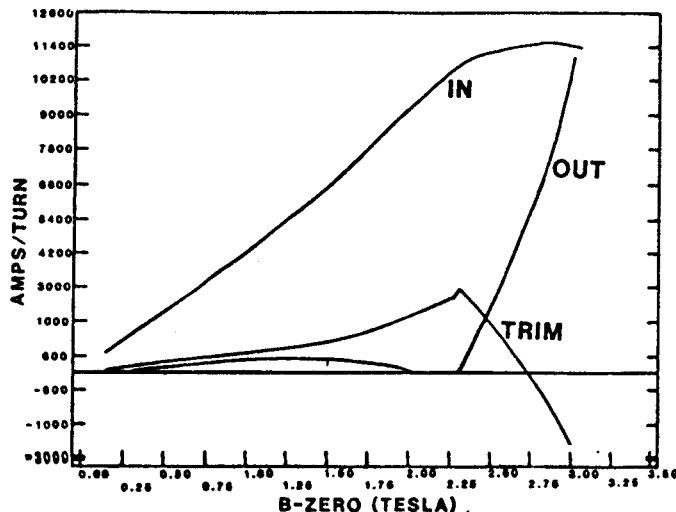
Figure 7: Excitation currents for the WF3CMS superferric dipole.

STORED ENERGY AND FORCES ON THE CONDUCTORS

The stored energy at 2.9889 Tesla is calculated to be 6.56 kJ/m. Table III gives the magnitude of the x and y components of force on the conductors. See figure 3 for the location of the various conductors. Note that the angle of the force, θ, is relative to the x axis.

Table III. Forces on the Conductors

Conductor	F_x(kg/m)	F_y(kg/m)	θ (degrees)
1	3687.0	-384.1	-3.4
2	2062.0	-465.3	-12.7
3	4448.0	-423.5	-5.4
4	1455.0	-623.0	-23.2
5	-736.1	-50.6	-176.1

LIMITATIONS OF THE NUMERICAL RESULTS

Field predictions based on numerical analysis are subject to many types of errors. Errors are induced by the discretization of the problem, round-off in the calculations and any deviations from reality in the assumed properties of the magnetic material. The latter is of considerable concern to us. For the field predictions we assumed that the iron was well represented by the magnetization curve for 1008 steel corrected to 4.2K[8]. The measurement of a magnetization curve is difficult to perform and at this time has not been completed on our steel, however, as will be seen later in this paper the agreement between predictions and measurements is pretty fair.

MAGNET ENDS

Magnet ends, where the current leads come in and out, the coils cross from one side to the other, and the tip and bottom coils are connected, are a potential source of problems. Besides requiring a substantial fraction of the magnet assembly labor, they may be the source of quenches due to conductor damage during cable bending, heat generated in connections between superconductor cables, potential cable immersion in high magnetic field regions, conductor movement if improperly supported, etc. The cable segments connecting left and right and up and down produce magnetic fields which may adversely affect the beam. The fewer ends, i.e., the fewer independently wound magnets the machine has, and the larger its circumference, the less the relative importance of ends.

Our present winding scheme is sketched in figure 8 for one independent coil, e.g., that carrying I_{in}. Its features are: (1) the input (1) and output (16) leads are

paired together so as to represent no net current outside
the magnet; (ii) the lead (12-13) carrying the current
from bottom to top is canceled by the output lead (16)
arranged to drop from top to bottom beside it before
exiting; (iii) the leads crossing left to right for the
downstream end of the upstreams magnet (eg. (13-14) and
(15-16)) are cancelled approximately by the leads crossing
right to left for the upstreams end of the adjacent
downstream magnet. In principle, then, the beam sees only
the dipole field of the windings inside the magnets. In
practice, the bottom to top and top to bottom connections
are wound in a spiral to reduce the sharpness of the bends
of the superconducting cable, and the cancellation is not
exact. Nevertheless preliminary field calculations using
MAGNUS and our first measurements, suggest that this
scheme produces end fields whose undesirable multipoles
are small enough as to have negligible effect on the beam.
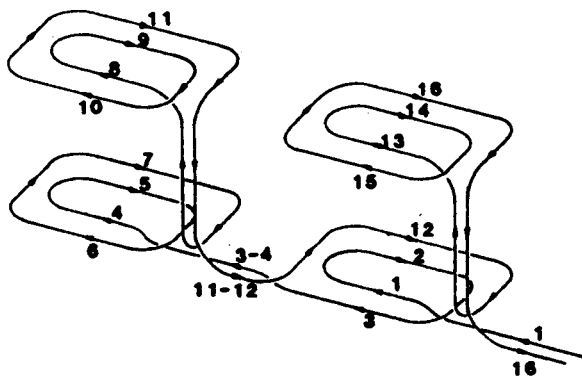
Figure 8:   End and Magnet-Winding Topology
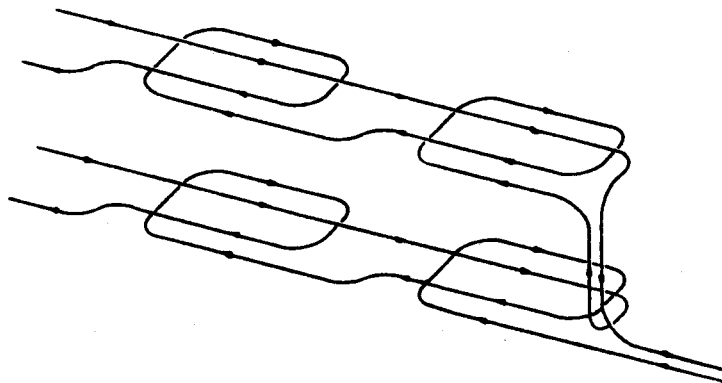
Figure 9:   A simpler winding possibility requiring twice
as many connections between superconducting cables.

Note that this scheme requires only the minimum possible number of superconducting connections per coil per magnet, i.e., one in (1) and one out (16) for an independent magnet, addition of (3-4) on to the next magnet in a string, and (11-12) coming back from it. Somewhat simpler windings are possible if, for example, four, rather than two, connections between magnets of a string are permitted (fig. 9).

In prototype magnets the end coils are wound in grooves machined in G10 blocks and clamped with matching blocks so as to be fixed rigidly in place. The end block structures do not extend laterally or vertically out beyond the cross-section of the magnet laminations, and extend only a few gap widths longitudinally beyond the magnet iron.

MAGNET CONSTRUCTION ERRORS

Large scale production of superferric magnets requires that strict tolerances be specified to the manufacturer. This requires in turn that potential sources of construction errors be identified, and the effect of each of them on the field quality be analyzed. Table IV defines the most important sources of error for the WF3CMS model. Also given are: the accuracy A with which the corresponding error can be controlled, and the RMS number of occurrences O per magnet:

Table IV. Sources of Error for the WF3ÇMS Model

HMIC	– Horizontal misplacement of each conductor of inner coil. $A = 25\mu m$, $O = \sqrt{8}$.
HMOC	– Horizontal misplacement of each conductor of outer coil. $A = 25\mu m$, $O = \sqrt{8}$
HMCC	– Horizontal misplacement of each conductor of correction coil. $A = 25\mu m$, $O = 2$.
VMIC	– Vertical misplacement of each conductor of inner coil. $A = 25\mu m$, $O = \sqrt{8}$
VMOC	– Vertical misplacement of each conductor of outer coil. $A = 25\mu m$, $O = \sqrt{8}$
VMCC	– Vertical misplacement of each conductor of correction coil. $A = 25\mu m$, $O = 2$.
GS	– Gap spacing. $A = 5\mu m$, $O = \sqrt{2}$ for b_n. $\sqrt{4}$ for B_o
CIN	– Current of inner coil. $A = 1A$, $O = 1$
COUT	– Current of outer coil. $A = 1A$, $O = 1$
CC	– Current in correction coil. $A = 0.2A$, $O = 1$.
MV	– μ variations. $A = 2\%$ at .15T, .18% at 3T, $O = 1$.
MM	– μ mismatch between the upper and the lower half of the magnet. $A = 2\%$ at .15T, .18% at 3T, $O = 1$.
SFV	– Stacking factor variations. $A = 0.1\%$, $O = 1$.
SFM	– Stacking factor mismatch between the upper and the lower half of the magnet. $A = 0.1\%$, $O = 1$.
SMV	– Shunt μ variations. $A = 2\%$ at .15T, .18% at 3T, $O = \sqrt{2}$.
SD	– Shunt displacement. $A = 25\mu m$, $O = \sqrt{2}$
STH	– Shunt thickness. $A = 25\mu m$, $O = \sqrt{2}$.

STI   - Shunt tilting. A = 25 µm, O = √2.
SG   - Shunt gap. A = 25µ, O = √2.
STM   - Shunt up/down thickness mismatch. A = 2µ, O = √2.

The sensitivity (defined as the partial derivative) of each multipole component with respect to each error was calculated using POISSON. In each case, a control case was solved and compared with an error case having an identical mesh. The results are reported in tables V and VI for field values of 0.15T and 3T, respectively, where all numbers have been rounded to the first decimal place, and S indicates values that are identically zero by the symmetry assumed in the calculation. Units in the tables are: B_0 is in gauss, harmonic coefficients are dimensionless, dimensions are in thousands of an inch (0.001 in ~ 25µm), currents are in KA, and variations of µ are in %. Sensitivities are given accordingly.

The corresponding induced random errors are obtained by multiplying the accuracy by the number of occurrences of each source and by the sensitivity of each harmonic. The results are given in table VII and VIII, which also show the total RMS error induced in each multipole component by the sources of errors. These last values are provisional because the contributions from a few error sources are still not known. Some of the missing contributions, however, have been computed for the WF2C model[9] and are believed to be approximately valid for the WF3CMS model. The total RMS errors in a_1 at 0.15T and in b_1 at 3T, are somewhat larger than we would like. The former is caused mainly by µ mismatch and by the vertical misplacement of the inner main coils. The latter, by shunt µ variations. All three parameters can, and will in the future, be controlled more tightly so that the design specifications are met.

Table V. Error sensitivities at 0.15T. Units and
nomenclature are described in the text.

Source of Error	B_0	b_2	b_4	b_6	b_1	b_3	b_5	a_1	a_3	a_5	a_2	a_4	a_6
HMIC	0.0	-0.1	0.0	0.0	S	S	S	-0.1	-0.1	0.0	S	S	S
HMOC	0.0	0.0	0.0	0.0	S	S	S	0.0	0.0	0.0	S	S	S
HMCC	0.0	0.1	0.0	0.0	S	S	S	-0.1	0.0	0.0	S	S	S
VMIC	0.0	-0.1	-0.1	0.0	S	S	S	0.5	0.1	0.0	S	S	S
VMOC	0.0	0.0	0.0	0.0	S	S	S	0.0	0.0	0.0	S	S	S
VMCC	0.0	-0.1	0.0	0.0	S	S	S	0.1	0.0	0.0	S	S	S
GS	-1.5	0.3	0.2	0.0	S	S	S	-1.9	-0.5	0.0	S	S	S
CIN	1980	57	30	6.1	S	S	S	S	S	S	S	S	S
COUT	1970	-170	-90	-19	S	S	S	S	S	S	S	S	S
CC	977	-229	-121	-25	S	S	S	S	S	S	S	S	S
MV	0.1	0.0	0.0	0.0	S	S	S	S	S	S	S	S	S
MM	0.0	0.0	0.0	0.0	S	S	S	0.0	0.0	0.0	S	S	S
SFV	0.0	0.0	0.0	0.0	S	S	S	S	S	S	S	S	S
SFM	0.0	0.0	0.0	0.0	S	S	S	0.0	0.0	0.0	S	S	S
SMV	0.0	0.1	0.0	0.0	0.0	0.0	0.0	S	S	S	S	S	S

	B_0	b_2	b_4	b_6	b_1	b_3	b_5	a_1	a_3	a_5	a_2	a_4	a_6
SD	0.0	0.1	0.0	0.0	S	S	S	S	S	S	S	S	S
STH	0.0	0.0	0.0	0.0	0.0	0.0	0.0	S	S	S	S	S	S
STI	S	S	S	S	S	S	S	1.1	0.2	-0.1	S	S	8
SG	0.0	0.2	0.1	0.0	S	8	S	-0.6	-0.1	0.0	S	S	8
STM	0.0	-0.3	-0.2	0.0	S	S	S	-11.6	-3.3	-0.5	8	8	S

Table VI.   Error sensitivities at 3T .   Units and
momenclature are described in the text

Source of Error	B_0	b_2	b_4	b_6	b_1	b_3	b_5	a_1	a_3	a_5	a_2	a_4	a_6
HMIC	-0.4	-0.1	0.0	0.0	S	S	S	-0.1	-0.1	0.0	S	S	S
HMOC	-0.2	0.1	0.0	0.0	S	S	S	-0.1	0.0	0.0	S	S	S
HMCC	-0.2	0.0	0.0	0.0	S	S	S	0.1	0.0	0.0	S	S	S
VMIC	-0.4	-0.1	0.0	0.0	S	S	S	0.3	0.1	0.0	S	S	S
VMOC	-0.9	-0.1	0.0	0.0	S	S	S	0.0	0.0	0.0	S	S	S
VMCC	0.2	0.1	0.0	0.0	S	S	S	0.0	0.0	0.0	S	S	S
GS	-8.6	0.2	0.1	0.0	S	S	S	-1.2	-0.1	0.0	S	S	S
CIN	960	26	3.6	0.4	S	S	S	S	S	S	S	S	S
COUT	760	0.7	-2.3	0.4	S	S	S	S	S	S	S	S	S
CC	470	0.9	-4.1	-1.2	S	S	S	S	S	S	S	S	S
MV	34	-0.5	-0.1	0.0	S	S	S	S	S	S	S	S	S
MM	17	-0.2	-0.1	0.0	S	S	S	2.1	0.2	0.0	S	S	S
SFV	163	3.0	-0.4	-0.1	S	S	S	S	S	S	S	S	
SFM	82	-1.7	-0.2	0.0	S	S	S	10.7	0.7	0.0	S	S	S
SMV	-5.0	-0.4	0.0	0.0	-0.9	-0.1	0.0	S	S	S	S	S	S
SD	-0.4	0.2	0.0	0.0	S	S	S	S	S	S	S	S	S
STH	-2.3	-0.1	0.0	0.0	-0.2	-0.1	0.0	S	S	S	S	S	S
STI	S	S	S	S	S	S	S	0.1	0.0	0.0	S	S	S
SG	0.0	0.0	0.0	0.0	S	S	S	-0.1	0.0	0.0	S	S	S
STM	-1.7	-0.2	0.0	0.0	S	S	S	-0.5	-0.2	-0.1	S	S	S

Table VII.   Induced errors at 0.15T

Source of Error	B_0	b_2	b_4	b_6	b_1	b_3	b_5	a_1	a_3	a_5	a_2	a_4	a_6
HMIC	0.0	-0.28	0.0	0.0	0.0	0.0	0.0	-0.28	-0.28	0.0	0.0	0.0	0.0
HMOC	0.0	0.0	0.0	0.0	0.0	0.0	0.0	0.0	0.0	0.0	0.0	0.0	0.0
HMCC	0.0	0.0	0.2	0.0	0.0	0.0	0.0	0.0	-0.2	0.0	0.0	0.0	0.0
VMIC	0.0	-0.28	-0.28	0.0	0.0	0.0	0.0	1.4	0.28	0.0	0.0	0.0	0.0
VMOC	0.0	0.0	0.0	0.0	0.0	0.0	0.0	0.0	0.0	0.0	0.0	0.0	0.0
VMCC	0.0	-0.2	0.0	0.0	0.0	0.0	0.0	0.2	0.0	0.0	0.0	0.0	0.0
GS	-0.6	0.09	0.06	0.0	0.0	0.0	0.0	-0.54	-0.2	0.0	0.0	0.0	0.0
CIN	1.98	0.06	0.03	0.0	0.0	0.0	0.0	0.0	0.0	0.0	0.0	0.0	0.0
COUT	1.97	-0.17	-0.09	0.0	0.0	0.0	0.0	0.0	0.0	0.0	0.0	0.0	0.0
CC	0.20	-0.05	-0.03	0.0	0.0	0.0	0.0	0.0	0.0	0.0	0.0	0.0	0.0
MV	0.2	0.0	0.0	0.0	0.0	0.0	0.0	0.0	0.0	0.0	0.0	0.0	0.0
MM	0.0	0.0	0.0	0.0	0.0	0.0	0.0	0.0	0.0	0.0	0.0	0.0	0.0
SFV	0.0	0.0	0.0	0.0	0.0	0.0	0.0	0.0	0.0	0.0	0.0	0.0	0.0
SFM	0.0	0.0	0.0	0.0	0.0	0.0	0.0	0.0	0.0	0.0	0.0	0.0	0.0
SMV	0.0	0.28	0.0	0.0	0.0	0.0	0.0	0.0	0.0	0.0	0.0	0.0	0.0
SD	0.0	0.14	0.0	0.0	0.0	0.0	0.0	0.0	0.0	0.0	0.0	0.0	0.0

```
STH     0.0 0.0 0.0 0.0 0.0 0.0 0.0 0.0 0.0 0.0 0.0 0.0 0.0
STI     0.0 0.0 0.0 0.0 0.0 0.0 0.01.56 0.28-0.140.00.0 0.0
SG      0.0 0.060.030.0 0.0 0.0-0.17-0.030.00.0 0.0 0.0
STM     0.0-0.04-0.030.00.0 0.0 0.0-1.64-0.47-0.0710.00.0.0
RMS
error 2.870.620.310.00.00.0 0.0 2.75 0.73 0.16 0.0 0.0 0.0
```

Table VIII: Induced Errors at 3T

Source of Error	B_0	b_2	b_4	b_6	b_1	b_3	b_5	a_1	a_3	a_5	a_2	a_4	a_6
HMIC	-1.13	-0.28	0.0	0.0	0.0	0.0	0.0	-0.28	-0.28	0.00	0.0	0.0	0.0
HMOC	-0.57	0.28	0.0	0.0	0.0	0.0	0.0	-0.28	0.0	0.00	0.0	0.0	0.0
HMCC	-0.4	0.0	0.0	0.0	0.0	0.0	0.0	-0.2	0.0	0.0	0.0	0.0	0.0
VMIC	-1.13	-0.28	0.0	0.0	0.0	0.0	0.0	0.85	0.28	0.00	0.0	0.0	0.0
VMOC	-2.5	-0.28	0.0	0.0	0.0	0.0	0.0	0.0	0.0	0.0	0.0	0.0	0.0
VMCC	0.4	0.2	0.0	0.0	0.0	0.0	0.0	0.0	0.0	0.0	0.0	0.0	0.0
GS	-3.4	0.06	0.03	0.0	0.0	0.0	0.0	-0.34	-0.03	0.00	0.0	0.0	0.0
CIN	0.96	0.03	0.0	0.0	0.0	0.0	0.0	0.0	0.0	0.0	0.0	0.0	0.0
COUT	0.76	0.0	0.0	0.0	0.0	0.0	0.0	0.0	0.0	0.0	0.0	0.0	0.0
CC	0.47	0.0	0.0	0.0	0.0	0.0	0.0	0.0	0.0	0.0	0.0	0.0	0.0
MV	6.12	-0.09	-0.02	0.0	0.0	0.0	0.0	0.0	0.0	0.0	0.0	0.0	0.0
MM	3.06	-0.04	-0.02	0.0	0.0	0.0	0.0	0.38	0.04	0.0	0.0	0.0	0.0
SFV	16.3	0.3	-0.04	-0.01	0.0	0.0	0.0	0.0	0.0	0.0	0.0	0.0	0.0
SFM	8.2	-0.17	-0.02	0.0	0.0	0.0	0.0	1.07	0.07	0.0	0.0	0.0	0.0
SMV	-1.27	-0.1	0.0	0.0	-0.23	-0.03	0.0	0.0	0.0	0.0	0.0	0.0	0.0
SD	-0.57	0.28	0.0	0.0	0.0	0.0	0.0	0.0	0.0	0.0	0.0	0.0	0.0
STH	-3.25	-0.14	0.0	0.0	-0.28	-0.14	0.0	0.0	0.0	0.0	0.0	0.0	0.0
STI	0.0	0.0	0.0	0.0	0.0	0.0	0.0	0.14	0.0	0.0	0.0	0.0	0.0
SG	0.0	0.0	0.0	0.0	0.0	0.0	0.0	-0.14	0.0	0.0	0.0	0.0	0.0
STM	-0.24	-0.03	0.0	0.0	0.0	0.0	0.0	-0.07	-0.03	-0.020	0.00	0.0	0.0
RMS error	20.37	.77	.061	.010	.36	0.14	.01	.54	.41	.02	.0	.0	0.0

MEASUREMENTS

We have measured two bores of the NF2C type, two bores of the WF2C type, and 6 bores of the WF3CMS type.

We measure the field shape by using a method developed at Brookhaven National Laboratory. This consists of measuring the induced EMF in a rotating coil inside the magnetic field and Fourier analyzing the signals to get harmonic content. Our probe, which was built by BNL consists of 4 coils as described in Table IX. Attached to the probe is a shaft encoder, which triggers a set of digital voltmeters to measure the voltages from the four different coils as shown in figure 10. The data is then read into a computer, where each of the signals are Fourier transformed. We can then combine the coefficients from the different coils to buck out the dipole components of the signal. Since the coils are arranged at different

phase angles, this algorithm also will eliminate the
effect of torsional vibrations.

Table IX   Geometry of Measurement Coils

Coil	Length	Radius	Turns	Start	Subtended
1	121.9cm	7.50mm	2	0.25°	180°
2	121.9cm	7.50mm	2	12.12°	180°
3	121.9cm	7.47mm	10	9.28°	12°
4	30.6cm	7.39mm	20	185.37°	12.2°
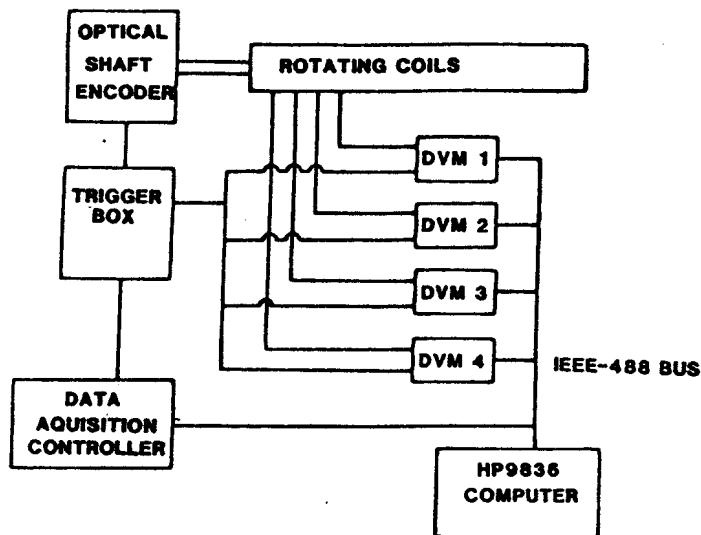
Figure 10:   Data Acquisition System

Since the multipole coefficients are measured by coil 4 at
R=0.739 cm, but reported at R=1 cm, the coefficients must
be scaled by $(1/0.739)^n$ for the nth multipole (e.g., $b_{10}(1$
cm) = 20.6 x $b_{10}(0.739$ cm)).   When the probe is running
smoothly, it can measure the low order multipoles to a few
parts in 10^5.   The probe gives us the absolute field to
less than 0.5%.

If the absolute field in 100m of dipole with a
bending radius of 22 km, varies by 0.5% the sagitta
changes by 1.1 mm. This means that we need a
reproducibility of B_0, from magnet to magnet of about
0.5%.   The field at Injection is 0.15 T, which is well
above the realm where the demagnetization of domains
produces random field errors.

Figure 11 shows the distribution of forbidden
multipoles from 6 different magnets, where we have
adjusted the current ratios to give $|b_2| < 10^{-4}$.   Table X

compares the RMS values of these distributions with other
types of dipoles. We give the multipoles for each magnet
style as they would be measured at a radius of 2/3 of the
radius of the beam pipe, rather than at 1 cm. This
roughly cancels the effect of scaling the magnet to a
smaller size. The worst distribution for superferrics is
that of the skew quadrupole, which is comparable to the
a_1 distribution from the other magnets. Skew quadrupole
is caused by a vertical shift of conductors relative to
the midplane between pole faces and by μ variations.

We have not included b_2 and b_4 in table X because
they are dependent on the style of pole face and the
current ratios. RMS values for b_2 and b_4 are probably
no worse than the distribution for a_2 and a_4, respectively
(i.e., ~ 1×10^{-4}). Comparison of data from 3 magnets
under identical conditions gives $\sigma(b_2) = 0.6$, $\sigma(b_4) = 0.5$
and $\sigma(b_6) = 0.2$. Measurements of multipoles for the 3
magnets are shown in Figures 12, 13, and 14. ·
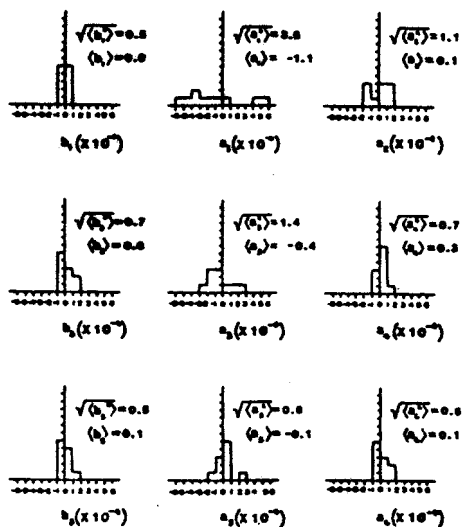
Figure 11. Distribution of Forbidden Multipoles

Table X. RMS multipole widths for dipoles of other machines
(R = 2/3R conductor)

	Tevatron	CBA	HERA I	HERA II	SACLAY	TAC R_o=1cm
Aperture:	3''	5.2''	3''	3''	4''	
magnets:	>700	15	2	4	3	6
b_1	1.9	1.0	2.3	2.2	2.0	1.2
a_1	2.9	2.8	4.3	2.4	2.9	3.6
b_2	3.1	2.4	~1.0	2.2	1.8	~1
a_2	1.2	0.4	0.3	0.8	0.7	1.1
b_3	0.8	0.2	0.8	1.1	1.2	0.7
a_3	1.5	1.3	0.6	2.5	0.9	1.4
b_4	1.3	1.1	1.4	1.0	1.3	~1
a_4	0.5	0.2	0.3	0.6	0.9	0.7
b_5	0.3	---	0.4	0.3	---	0.5
a_5	0.6	---	0.8	1.5	---	0.6
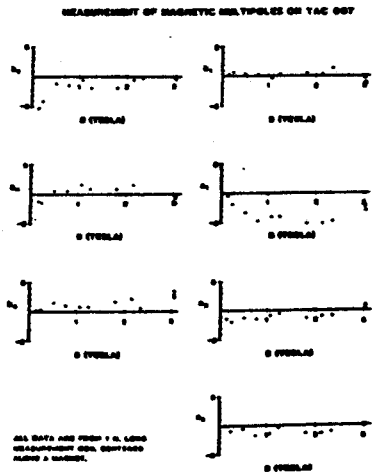
Figure 12: Measurement of Magnetic Multipoles on TAC7

Figure 13: Measurement of Magnetic Multipoles TAC9
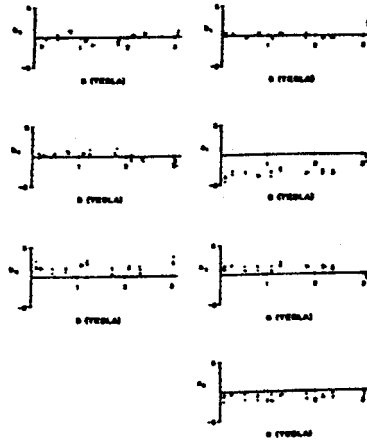
Figure 14. Measurement of Magnetic Multipoles on TAC10

COMPUTER SOFTWARE

Since the superferric dipole is very long compared to the dimensions of its cross-section most of the calculations are two-dimensional. The programs POISSON and CUARM2 were used for all two-dimensional calculations. POISSON is a finite difference program that solves problems of nonlinear magnetostatics using the vector potential as the unknown. Field components, forces, field harmonics and stored energy can also be computed. The program has been used for a number of years in several countries, and is considered as a standard. We found, however, that the results from POISSON can be affected by large errors [7] in the particular case of superferric magnet design, where magnetization tables with no more than 30 or 40 points are commonly used. The interpolation relations employed by POISSON are inappropriate in such cases. We proposed the use of better interpolation relations, and generated a magnetization table for 1008 steel at 4.2K with 200 points [8] , so that now the magnetic properties of the material can be accurately represented. Even though final measurements of magnetization for the specific steel used for the construction of the prototypes are not yet available, the errors between predictions and measurements are now well below 0.1% in all cases, as reported.

The program CUARM2 [10] can solve the quasi-harmonic equation in nonlinear cases, using the finite element method, in two dimensions. It can thus be used for the solution of problems of nonlinear two-dimensional magnetostatics with the vector potential as the main unknown. This program is much more accurate than POISSON, and consequently it played an essential role when very accurate calculations were required for the analysis of crenellation [3] . This analysis showed that crenellation

would not be appropriate for the design of the SSC, and led to the conclusion that there is going to be no crenellated SSC.

Calculations associated with the design of the ends of the magnet are essentially three-dimensional. They were solved using the program MAGNUS [4,5,11]   . This is a finite element program for problems of three-dimensional nonlinear magnetostatics. It uses the well known and accurate two-scalar-potentials method. End design is currently in progress and not many results are available. The following table shows a comparison between results of MAGNUS and POISSON and measured values for a two-dimensional case, the WF3CMS:

	$B_0(T)$	b_2	b_4	b_6
MEASURED	2.9812	-34.4	-14.9	0.4
MAGNUS	2.9863	-34.3	-14.8	-0.4
POISSON	3.0076	-35.2	-16.0	-0.6

The harmonic components are given in parts in 10^4, as usual. The error in B_0 is 0.17% for MAGNUS and 0.89% for POISSON. Measurements are believed to be accurate within 0.5% for fields and 0.4 part for harmonic components. The agreement is satisfactory, and shows that MAGNUS is more accurate than POISSON, as expected.

CONCLUSIONS

The WF3CMS (wide face with three currents and a magnetic shunt) superferric dipole is simple to build, reliable and cost effective. It can produce the desired uniform magnetic field in the range 0.15 to 3T in a 2.5 x 3.7 cm bore. It can be industrially produced because tolerances specified for all design parameters are acceptable. The WF3CMS superferric is a very good option for the SSC.

REFERENCES

1. P. R. Huson, P. VanderArend, H. Hinterberger, P. Mantsch, A.McInturf and S. Snowdon, Design of Superferric Magnets for a Multi-TeV storage ring, in ''Proc. 12th Int. Conf. on High Energy Accelerators,'' Fermilab (1983).

2. P. R. Huson, W. Schmidt and S. Pissanetzky, ''Transverse Crenellation of Dipole Magnets,'' Report TAC -284-10, Texas Accelerator Center (1984).

3. S. Pissanetzky, Design of Crenellated Magnets, Nuclear Instr. and Methods in Physics Research, B10/11, 799-801 (1985).

4. S. Pissanetzky, The Design of Superferric Magnets for the Superconducting Supercollider and the New Program MAGNUS for Three-Dimensional Magnetostatics in ''Proc. Conf. on the Computation of Electro-Magnetic Fields (COMPUMAG),'' Fort Collins, Colorado, June 3-6 (1985).

5. S. Pissanetzky, Solution of Three-Dimensional Anisotropic Nonlinear Problems of Magnetostatics Using Two Scalar Potentials, Finite and Infinite Multipolar Elements and Automatic Mesh Generation. I.E.E.E. Trans. on Magnetics, Vol. MAG-18, P.346-350 (1982).

6 J. Herrera et al., Magnetic Field Measurements of Superconducting Magnets for the Colliding Beam Accelerator, in: ''Proc. 12th, Int. Conf. on High-Energy Accelerators'', Fermilab, Aug. 11-16 (1983), p.563-568.

7. S. Pissanetzky, The Interpolation of Magnetization Tables and the Program POISSON, Report TAC-1104/85, Texas Accelerator Center (1985).

8. R. Carcagno and S. Pissanetzky, A Smooth Magnetization Table for 1008 Steel at 4.2 K, Report TAC-257/85, Texas Accelerator Center (1985).

9. S. Pissanetzky and W. Schmidt, ''Design of the Dipole Magnet for the C Version of the Superconducting Supercollider 20 TeV Twin-Beam Proton Accelerator (SSC), in Proc. 1985 Particle Accelerator Conf., Vancouver, May 13-16 (1985).

10. S. Pissanetzky, Private Communication.

11. S. Pissanetzky, ''MAGNUS. Computer-Aided Design of Electromagnets'', Brookhaven National Laboratory, report BNL 28416, AMD 867 (1980).